

Supporting Information for: Taming thermodiffusive transport of alkali halide solutions confined in silica nanopores[†]

Silvia Di Lecce, Tim Albrecht, and Fernando Bresme

1 Simulation details

The following procedure was used to build the amorphous silica nanopore. First, we generated a small crystal of silicon dioxide, SiO₂, using the Inorganic Builder tool of VMD¹. The orthogonal parallelepiped crystal with dimensions 5.48 nm × 5.48 nm × 6.25 nm, consisted of 4356 Si and 8712 O atoms and 1089 unit cells, and it was equilibrated for 1 ns in the NVT *ensemble*, at 300 K. We applied a series of temperature cycles to melt the crystal by increasing the temperature up to T = 5000 K at a rate of 25 K ns⁻¹. Then we performed a series of quenching cycles to set the temperature to 300 K at a rate of 20 K ps⁻¹, following ref.². The quenching rate does not lead to a different bulk density, however it has an impact on the number of defects observed in the final structure. The higher the rate the larger the density of structural defects³.

atom type	mass [au]	σ [Å]	ϵ [kJ mol ⁻¹]	q [e]
Si	28.080	3.0203	7.7005×10^{-6}	+2.10
O	15.9994	3.16556	0.65017	-1.05
O _{OH}	15.9994	3.16556	0.65017	-0.95
H _{OH}	1.0	2.350	0.0	+0.425

Table 1 Lennard Jones parameters describing the interactions between the molecules of the silica nanopore. We used the CLAYFF model to describe the silanol groups (subscript OH) and ASiO₂⁴.

We used the CLAYFF model⁴, which is widely employed to model silica–water interactions^{3,5–9}. Numerical values of the force field parameters used for the silica nanopore are given in Table 1. More information on the silica structure can be found in the Supporting Information. Water was modelled using SPC/E water model¹⁰, and the ion–ion and ion–water interactions with the model described by Dang et al.^{11–14}.

To make the cylindrical nanopore the ASiO₂ block was cut following the procedure described in ref.³. We removed all Si atoms inside the pore region (1.5 or 2.0 nm from the pore axis) and all the O atoms that were not coordinated to at least one Si atom. Particular attention must be taken when considering the silica substrate surface in contact with aqueous solutions. Previous studies showed that the hydroxylation of amorphous silica surface is of critical importance to mimic realistically the silica–solution interactions¹⁵. The silanol groups form at the surface through two main processes: during the silica synthesis and in presence of water or aqueous solutions as a result of rehydroxylation of silica. Given our interest in aqueous solutions, the OH groups were included in our model of amorphous silica. The H atoms were attached randomly to singly–coordinated O atoms. This resulted in a interface containing isolated silanols Si(OH), geminal silanols Si(OH)₂ and Si(OH)₃. To maintain electroneutrality we adjusted the charge by randomly adding or removing H atoms. The final ASiO₂ surface is shown in Fig. S3 of the SI.

The pore was subsequently filled with SPC/E water. The system was equilibrated for 10 ns at 300 K. During the first 3 ns the water molecules interact with the solid surface also diffusing into the ASiO₂ structure. The ability of water to penetrate and diffuse into the solid structure is connected to both silanol groups, the roughness of the surface, which enhances the hydrophilicity of the ASiO₂ nanopore, and the presence of structural defects, namely oxygen atoms or silicon vacancies. We found that water did not completely penetrate into the structure, and the amount of water inside the glass remained constant after 10 ns (see Fig. S4 in the SI for further details). The simulations reported in this article were performed with 10 set of nanopores, 5 independent configurations with radii 1.5 nm (R₁) and and 5 nanopores with radius 2 nm (R₂). The cumulative simulation time is 2–4 μ s.

LiCl and NaCl ions at 1 mol kg⁻¹ concentration, were added to the nanopores. We carefully checked that no cation or anion were placed into the ASiO₂ structure. The entire systems were equilibrated for 10 ns at 300 K. Subsequently, we replicated the systems the z -direction and equilibrated for another 5 ns. The temperature gradient was then applied and the first 50 ns were neglected in the analysis of the thermodiffusive response of the solutions. The box dimensions were $L_x \times L_y \times L_z = 5.48 \text{ nm} \times 5.48 \text{ nm} \times 24.0 \text{ nm}$ and the nanochannels were both 6.0 nm long.

The temperature profiles (see Fig. 3 (a) in the main text) were calculated by dividing the simulation box in small volumes of size $0.685 \text{ nm} \times 0.685 \text{ nm} \times 0.4 \text{ nm}$. The temperature was computed using the equipartition principle and the local kinetic energies. The Lennard–Jones interactions were truncated at a cut–off radius of $r_c = 1.5 \text{ nm}$. The coulombic forces were computed using the Particle Mesh Ewald method (PME)¹⁶, with a mesh width of 0.12 nm and an interpolation order of 4. From the mole fraction of salt and thermal gradients along the nanopore, we computed the Soret coefficient (see main text). We divided the system in 100 layers and discarded in our analysis in these calculations the layers within 0.6 nm from the openings of the nanopore.

1.1 Silica nanopore

Figure 1 shows the unit cell of crystalline silicon dioxide (left), the simulated system before the melting process in the crystalline structure (centre) and after the annealing cycles in the amorphous form (right). More details about the equilibration are discussed in the Methods section.

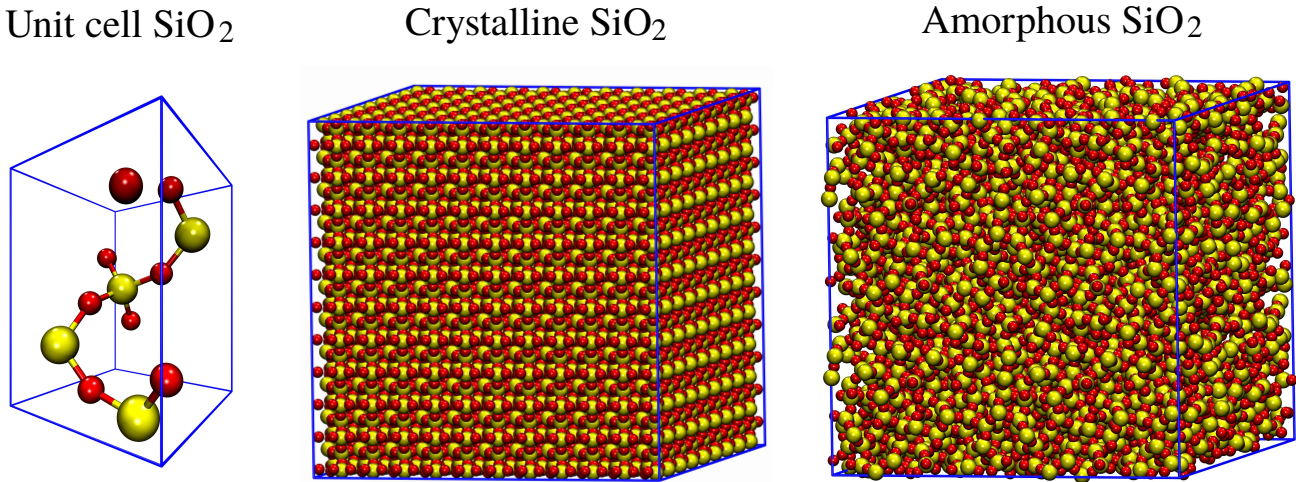


Fig.S 1 Unit cell employed to build the initial crystal of silicon dioxide.

The radial distribution functions of the site pairs Si–Si, Si–O and O–O of the quenched SiO₂ glass were calculated following a short equilibration of few nanoseconds at 300 K. The analysis lasted 100 ps. Figure 2 shows the radial distribution functions of the pairs, Si–O, O–O and Si–Si. The coordinates of the first peaks of these functions and the average density of the ASiO₂ are reported in Table 2. The experimental results refer to measured data using neutron diffraction.

	$\rho \text{ [kg m}^{-3}\text{]}$	$r_{\text{Si-O}} \text{ [nm]}$ 1 st peak	$r_{\text{O-O}} \text{ [nm]}$ 1 st peak	$r_{\text{Si-Si}} \text{ [nm]}$ 1 st peak	$r_{\text{Si-O}} \text{ [nm]}$ 2 nd peak
simulation ³	2150	0.157	0.255	0.3110	0.399
experiment ^{17,18}	2200	0.160	0.261	0.3115	0.413
this work	2243	0.154	0.252	0.3060	0.394

Table 2 Radial distribution function peak positions for ASiO₂. The experimental data were obtained from the neutron diffraction results by Ohno et al.¹⁷; the experimental density was reported by Hudon et al.¹⁸ and the simulation data were obtained from Bourg et al.³

The cylindrical nanopores were obtained as described in the Methods sections. Silanol groups were randomly added to the surface. Different types of silanol groups and siloxane bridges were obtained in the ASiO₂ surface (see Figure 3). Silanol, or OH groups, were classified as isolated, geminal, vicinal silanols (OH groups bounded through the hydrogen bond). Siloxane groups represent bridges with oxygens atoms on the surface.

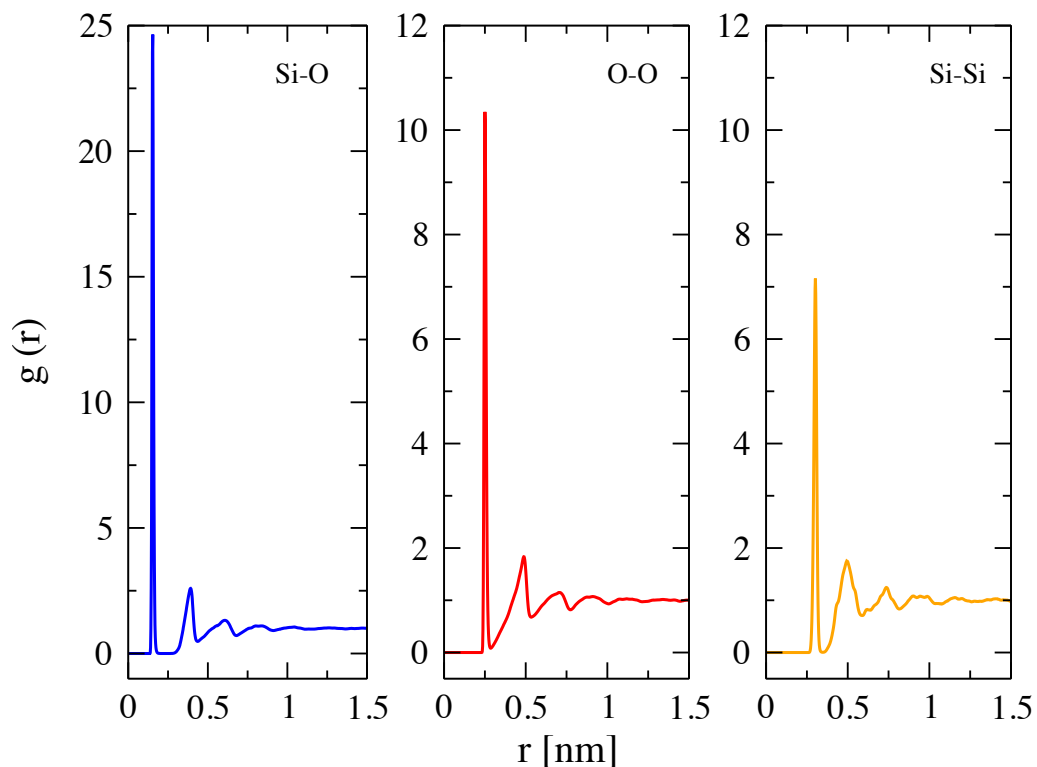


Fig.S 2 Silicon-Oxygen (left), Oxygen-Oxygen (centre) and Silicon-Silicon (right) radial distribution function at 300 K. The label in each plot indicate the site pairs.

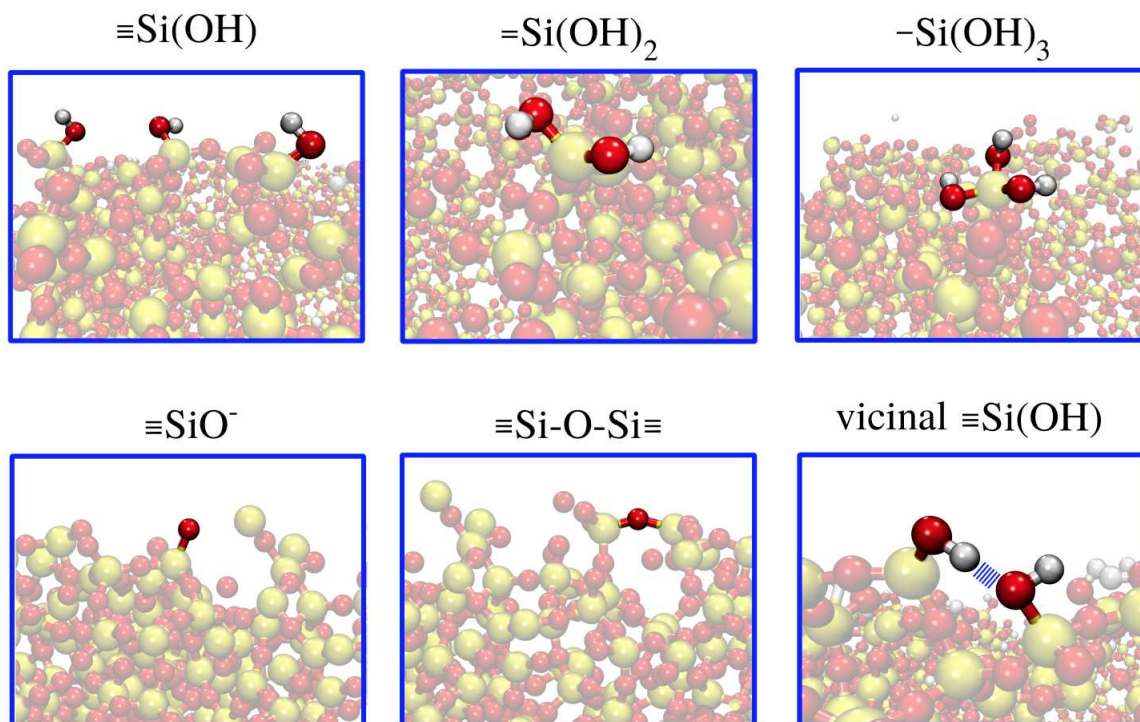


Fig.S 3 Types of groups formed at the silica surface. Isolated silanols $\equiv\text{Si}(\text{OH})$, geminal silanols $=\text{Si}(\text{OH})_2$ and $-\text{Si}(\text{OH})_3$. Dangling oxygens $\equiv\text{SiO}^-$, siloxane bridge $\equiv\text{Si}-\text{O}-\text{Si}\equiv$ and vicinal silanols, in which a hydrogen bond (dashed blue line) connects a pair of silanols. Oxygen, Silicon and Hydrogen atoms are indicated in red, yellow and white, respectively.

1.2 Equilibrium simulations of LiCl and NaCl confined in silica nanopores

Table 3 shows the number of atoms for the systems considered in this work.

atom type	R ₁ (R= 1.5 nm)	R ₂ (R= 2.0 nm)
Si	5364	3840
O	11988	8946
Si(OH) ₃	46	46
Si(OH) ₂	304	334
Si(OH) ₁	622	606
SOL	14582	16774
Li ⁺ / Na ⁺	247	400
Cl ⁻	247	400

Table 3 Number of atoms in the R₁ (R = 1.5 nm) and R₂ (R = 2.0 nm) nanopores. The silanol groups are indicated as Si(OH)_n and each group contains one Si, n atoms of O and H. The number of molecules of water is indicated as SOL.

After solvating the nanopore, as described in the Methods section, the system was equilibrated for 10 ns. Figure S4 shows typical snapshots at the start of the simulation (0 ns) and after 10 ns. In the first nanoseconds of equilibration, the water molecules penetrate into the ASiO₂, due to the interactions with the silanol groups and the roughness of the surface.

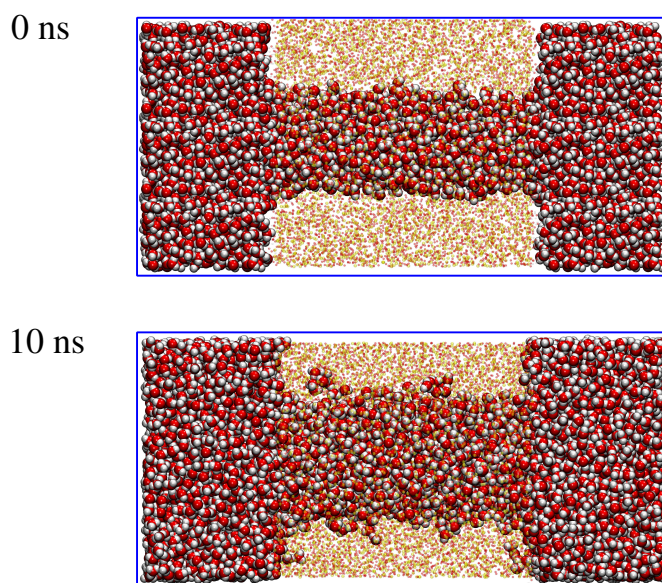


Fig.S 4 Representative snapshots of a nanopore of radius 1.5 nm filled with water at different times. The lower panel illustrates water penetration into the silica surface.

Additional equilibrium simulations were performed to analyse the structural properties of confined LiCl and NaCl aqueous solutions at 240 K and 360 K. We have analysed the last 5 ns of a production run at the wanted temperature and 600 bar. A comparison between the structural properties of bulk solutions (R_∞), and solutions confined between nanopore of radii R₁ = 1.5 nm and R₂ = 2.0 nm are shown in Fig. S5 and Fig. S6 for LiCl and NaCl aqueous solutions, respectively. We report the radial distribution functions and the coordination numbers at 240 K (a–f) and 360 K (g–k). OW and HW represent oxygen and hydrogen atoms of water molecules, O and H are oxygen and hydrogen at the silica surface, Li, Na and Cl represent the anion and cation of the solutions.

As for 300 K, confinement induces structural changes at both the temperature reported here. The radial distribution functions show different heights in their main peaks, whereas the position of the first maximum is independent of confinement. Dehydration of the water solvation shell around both anions and cations is observed when the solution is confined in narrower pores, independently of the average temperature used.

LiCl, 240K

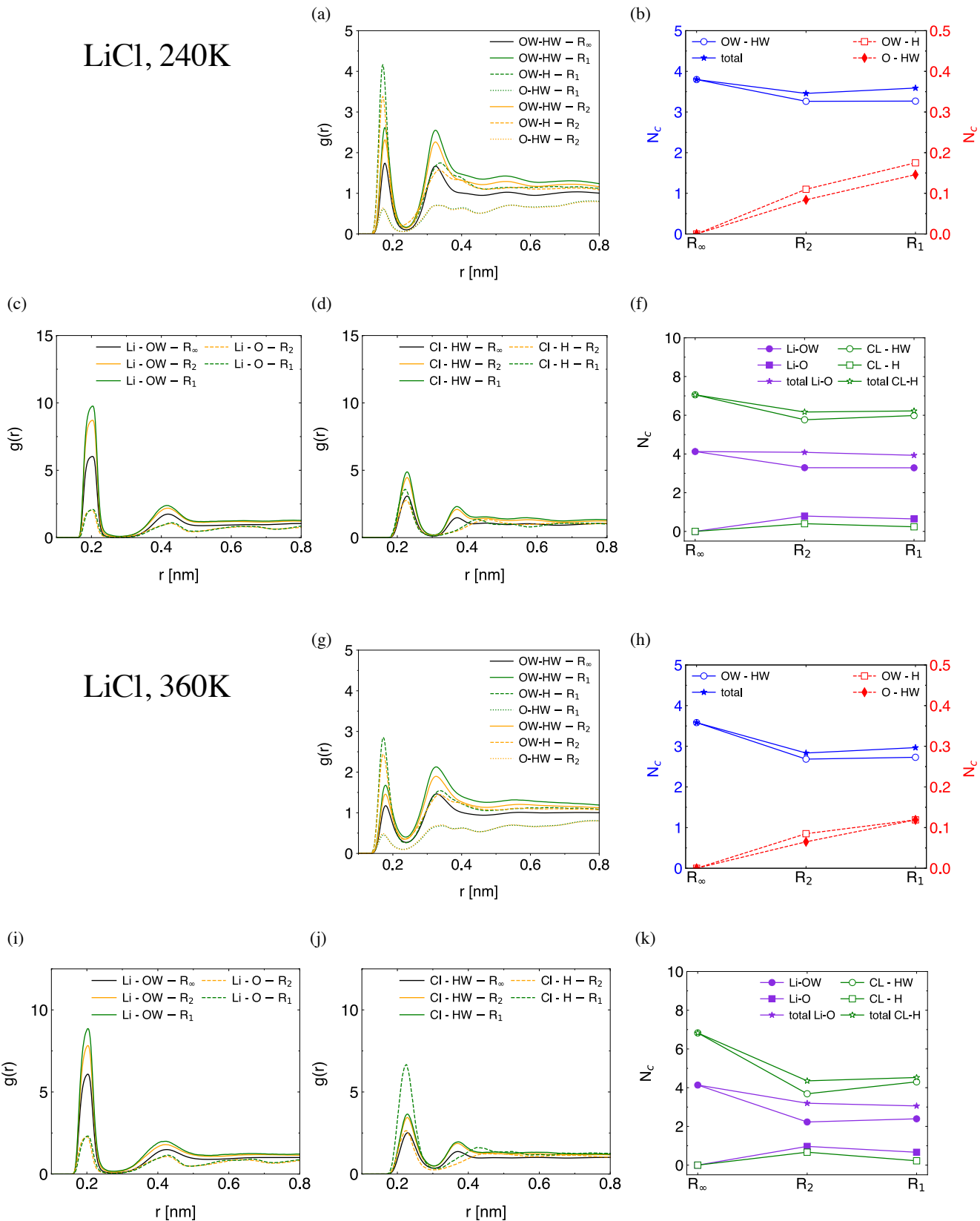


Fig.S 5 Comparison of the normalised radial distribution functions $g(r)$ and coordination numbers N_C for LiCl at 240K (a–f) and 360 K (g–k) aqueous solutions in bulk conditions (R_∞) and confined between nanopore of radii 1.5 nm (R_1) and 2.0 nm (R_2). OW and HW represent oxygen and hydrogen atoms of water molecules, O and H are oxygen and hydrogen at the silica surface. The radial distribution functions have been normalised using the value $g(r=1.5 \text{ nm})$.

NaCl, 240K

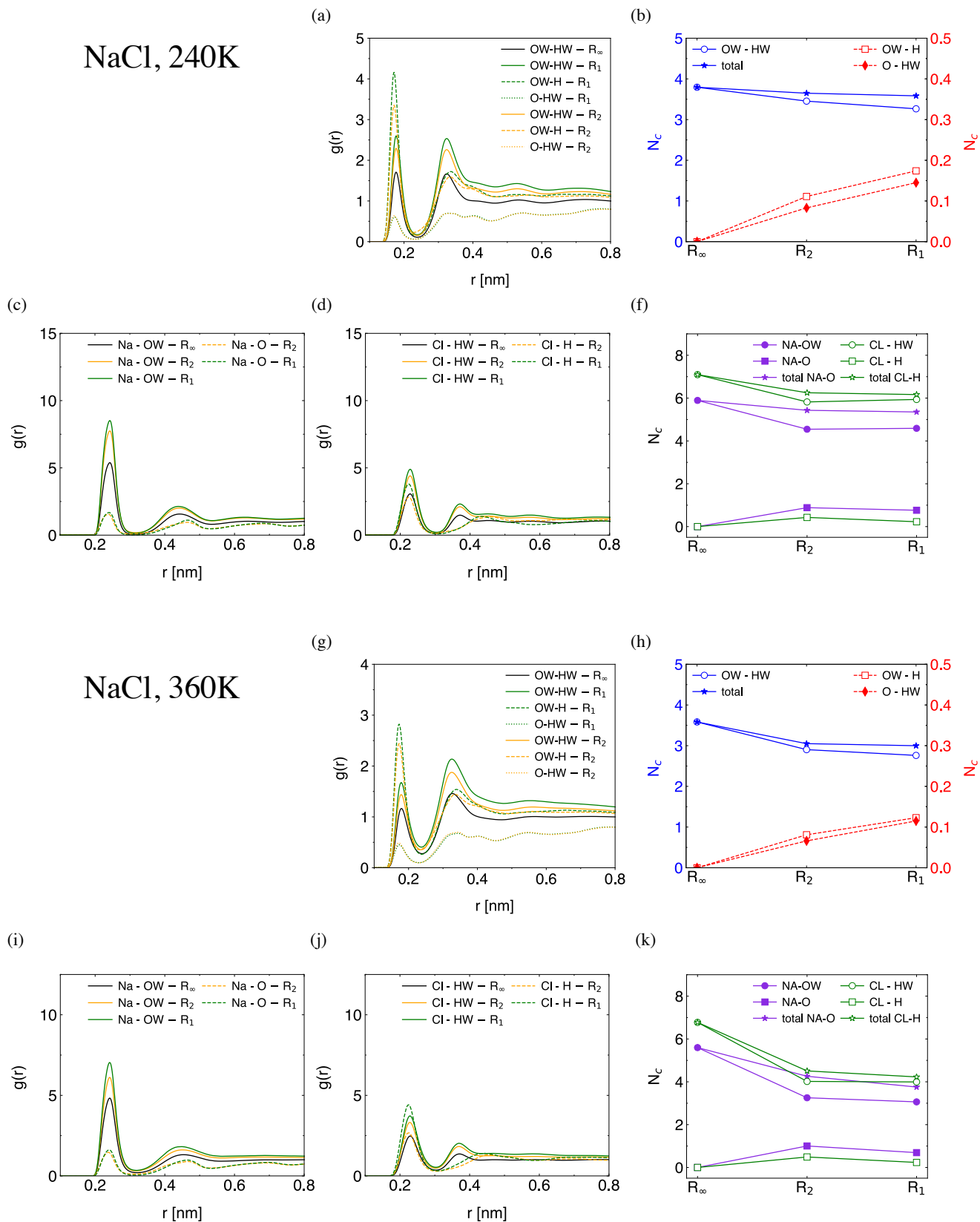


Fig.S 6 Comparison of the normalised radial distribution functions $g(r)$ and coordination numbers N_c for NaCl at 240K (a-f) and 360 K (g-k) aqueous solutions in bulk conditions (R_∞) and confined between nanopore of radii 1.5 nm (R_1) and 2.0 nm (R_2). OW and HW represent oxygen and hydrogen atoms of water molecules, O and H are oxygen and hydrogen at the silica surface. The radial distribution functions have been normalised using the value $g(r=1.5 \text{ nm})$.

2 Non-equilibrium simulations of LiCl and NaCl confined in silica nanopores

2.1 Average number of hydrogen bonds

We have extended our analysis by computing the average number of hydrogen bonds per water molecules inside the nanopore, as a function of their position inside the pore. With this calculation we assess the impact of the local environment, namely local temperature, on the structure of the solution.

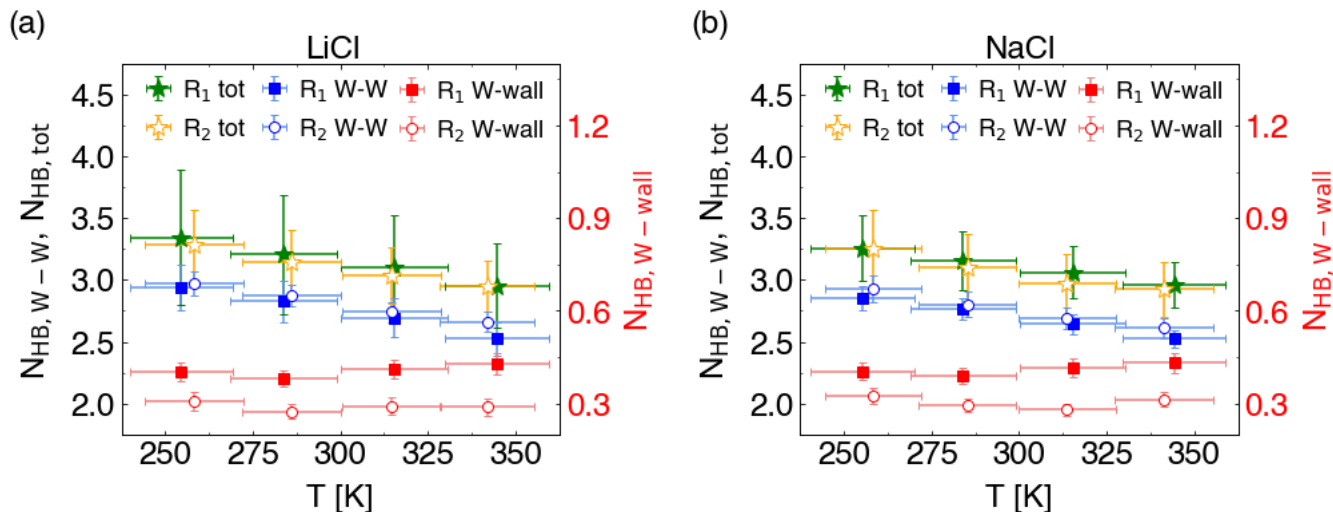


Fig.S 7 Average number of hydrogen bonds per water molecule between water molecules and water-silica for LiCl (a) and NaCl (b) solutions under confinements as a function of temperature. $N_{\text{HB},\text{W-W}}$ and $N_{\text{HB},\text{W-wall}}$ indicate the average number of hydrogen bonds per water molecule between water molecules and between water and silanol groups, respectively. $N_{\text{HB},\text{tot}} = N_{\text{HB},\text{W-W}} + N_{\text{HB},\text{W-wall}}$. The right y -axis in panels (a) and (b) shows $N_{\text{HB},\text{W-wall}}$ (red symbols), while the left y -axis $N_{\text{HB},\text{tot}}$ and $N_{\text{HB},\text{W-W}}$.

We computed the average number of hydrogen bonds (HB) per water molecule, between water molecules and between water and the silanol groups at the nanopore surface. All the data were obtained from analyses of trajectories covering the last 50 ns of the NEMD simulations. We consider that two molecules are hydrogen bonded if the oxygen-oxygen distance is < 0.35 nm and the angle between the vector connecting the oxygen atoms and the bond between the oxygen-oxygen and the oxygen-hydrogen covalent bond, vector is smaller than 30° . This criterion was applied to create hydrogen bonds, both between water molecules or between water and silanol groups. In Figure S7 (a, b) we compare the results obtained from our analysis. To take into account the temperature gradient, the nanopore was divided in 4 sampling-volumes of 1 nm thickness, neglecting the sampling volumes located at 1 nm from the entrance of the pore. The average number of HB between water molecules ($N_{\text{HB},\text{W-W}}$) decreases in the confined systems with respect to bulk, irrespective of the solution considered, NaCl or LiCl, or temperatures (see Table 2 and Figure S7 (a, b)). The average number of HB between water molecules and silanol groups ($N_{\text{HB},\text{W-wall}}$) features a weak dependence with temperature. The main message from these calculations is that the overall average number of HB ($N_{\text{HB},\text{tot}}$) decreases with temperature inside the nanopore. Water-water interactions are the main driving force behind the observed behaviour.

2.2 Ions pair correlation functions

We show in Figure S8 the anion–cation radial distribution functions for the confined solutions (NaCl and LiCl in nanopores with radii R_1 and R_2) under the thermal gradient.

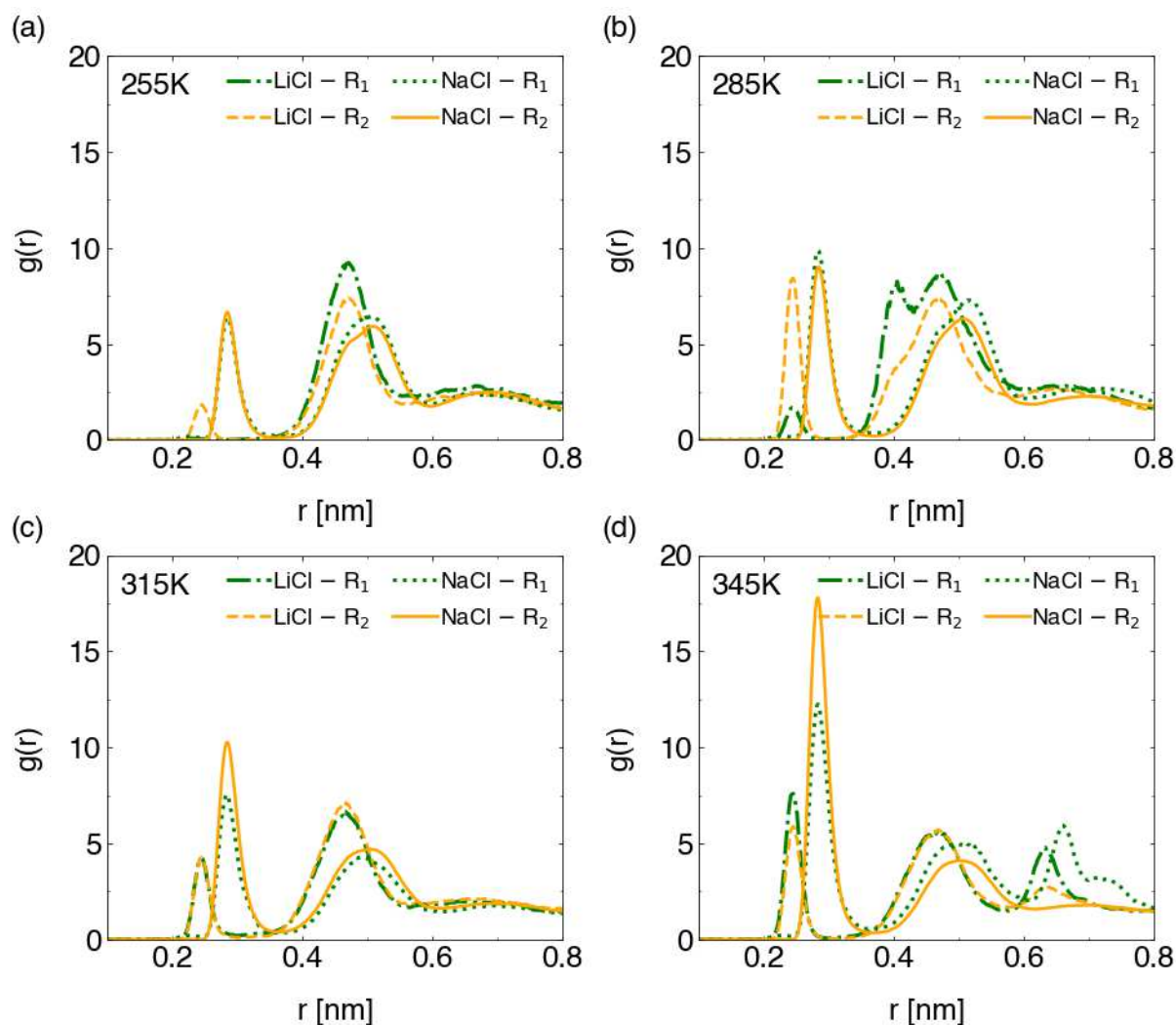


Fig.S 8 Comparison of the radial distribution functions $g(r)$ between anions and cations for confined LiCl or NaCl aqueous solutions (R_1 and R_2) under a thermal gradient, as a function of the pore axial position (or temperature). The radial distribution functions have been normalised using the value $g(r=1.5 \text{ nm})$.

The data were averaged over the last 50 ns of the simulation. The confined region was divided in 4 layers of 1 nm thickness, corresponding to 4 different temperatures, 255K (a), 285K (b), 315K (c) and 345K (d).

We computed the percentage of ion pairs as a function of the location of the ions inside the nanopore, to assess the impact that the thermal gradients have on the structure of the aqueous solutions, $\frac{N_c}{N_{\text{anion,cation}}} \times 100$ (see Figure S9 for definitions). For all the systems investigated the % of ion pairs is found to be rather small $< 3.5\%$ for NaCl and $< 0.8\%$ for LiCl. The level of ion pairing increases with confinement (*c.f.* R_1 and R_2 in Figure S9), for both LiCl and NaCl, while we do not find a clear dependence with temperature. Although the % of ion pairs is clearly higher when the solutions are under confinement conditions, the level of ion pairing remains small. Overall, we conclude that variation of ion pairing with temperature cannot explain the changes in the thermodiffusion behaviour reported in the main paper.

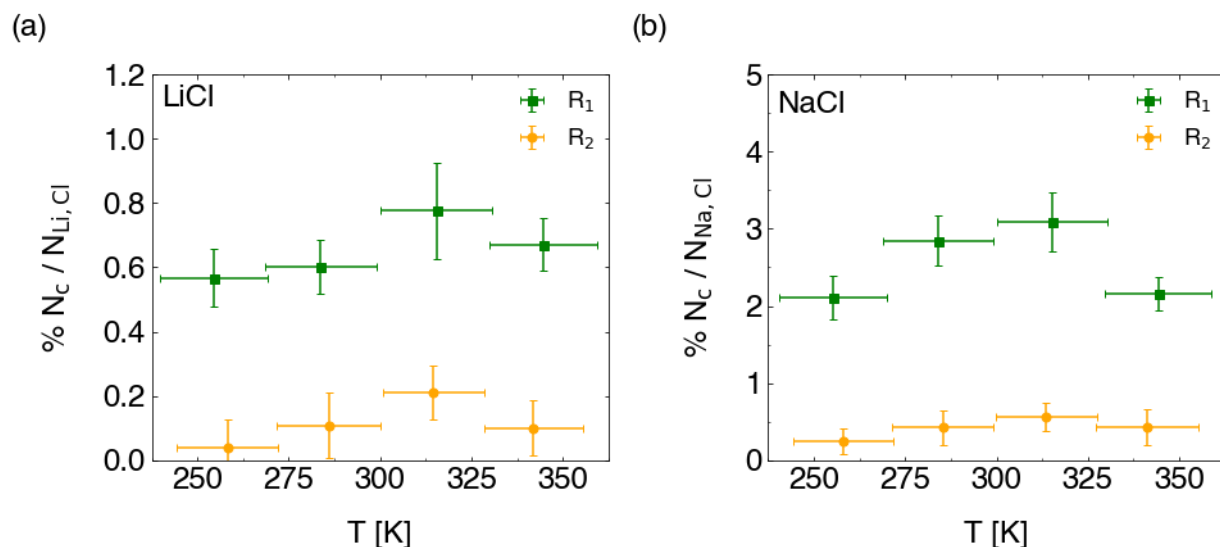


Fig.S 9 Percentage of ion pairs, $\frac{N_c}{N_{anion,cation}} \times 100$, as a function of temperature, for LiCl (a) and NaCl (b) aqueous solutions. N_c is the number of counter-ions around a given ion, in the first coordination shell (defined by the distance corresponding to the first minimum in the $g(r)$). $N_{anion,cation}$ is the average number of ions in the sampling volumes used in the NEMD simulations. R₁ and R₂ represent data for nanopores of different radii under a thermal gradient.

Notes and references

- 1 W. Humphrey, A. Dalke and K. Schulten, *J. Mol. Graph.*, 1996, **14**, 33.
- 2 E. Cruz-Chu, A. Aksimentiev and K. Schulten, *J. Phys. Chem. B*, 2006, **110**, 21497.
- 3 I. Bourg and C. Steefel, *J. Phys. Chem. C*, 2012, **116**, 11556.
- 4 R. Cygan, J.-J. Liang and A. Kalinichev, *J. Phys. Chem. B*, 2004, **108**, 1255.
- 5 A. Skelton, P. Fenter, J. Kubicki, D. Wesolowski and P. Cummings, *J. Phys. Chem. C*, 2011, **115**, 2076.
- 6 E. Ferrage, B. Sakharov, L. Michot, A. Delville, A. Bauer, B. Lanson, S. Grangeon, G. Frapper, M. Jiménez-Ruiz and G. Cuello, *J. Phys. Chem. C*, 2011, **115**, 1867.
- 7 V. Marry, E. Dubois, N. Malikova, S. Durand-Vidal, S. Longeville and J. Breu, *Environ. Sci. Technol.*, 2011, **45**, 2850.
- 8 M. Collin, S. Gin, B. Dazas, T. Mahadevan, J. Du and I. C. Bourg, *J. Phys. Chem. C*, 2018, **122**, 17764–17776.
- 9 C. D. Daub, N. M. Cann, D. Bratko and A. Luzar, *Phys. Chem. Chem. Phys.*, 2018, **20**, 27838–27848.
- 10 H. Berendsen, J. Grigera and T. Straatsma, *J. Phys. Chem.*, 1987, **91**, 6269.
- 11 L. Dang, *J. Chem. Phys.*, 1992, **96**, 6970.
- 12 L. Dang and B. Garrett, *J. Chem. Phys.*, 1993, **99**, 2972.
- 13 D. Smith and L. Dang, *J. Chem. Phys.*, 1994, **100**, 3757.
- 14 L. Dang, *J. Am. Chem. Soc.*, 1995, **117**, 6954.
- 15 L. Zhuravlev, *Colloids Surf., A*, 2000, **173**, 1.
- 16 T. Darden, D. York and L. Pedersen, *J. Chem. Phys.*, 1993, **98**, 10089.
- 17 H. Ohno, S. Kohara, N. Umesaki and K. Suzuya, *J. Non-Cryst. Solids*, 2001, **293**, 125.
- 18 P. Hudon, I.-H. Jung and D. Baker, *Phys. Earth Planet. Inter.*, 2002, **130**, 159.